Letters in Applied NanoBioScience
Open-Access Journal (ISSN: 2284-6808)

Article
Volume 14, Issue 3, 2025, 125
https://doi.org/10.33263/LIANBS143.125

Towards Semiconductor Hybrid Nanomaterials of Silicon/Germanium/Tin Oxide for Transport of Ions (Lithium/Sodium/Potassium) Across Cell Membrane

Fatemeh Mollaamin [1,*]

[1] Department of Biomedical Engineering, Faculty of Engineering and Architecture, Kastamonu University, Kastamonu, Turkey
* Correspondence: fmollaamin@kastamonu.edu.tr;

Received: 1.05.2025; Accepted: 17.07.2025; Published: 6.09.2025

Abstract: Germanium, tin/silicon-based nanoparticles are used as excipients in pharmaceutical technology. Recently, silicon/germanium oxide has emerged as a drug delivery system. Therefore, in this article, the promising alternative alkali metals of sodium-ion and potassium-ion delivery are discussed. This paper reports the presence of human cells of an additional ouabain-insensitive transport pathway for Li^+–Na^+ and Li^+–K^+ ions cotransport. A comprehensive investigation on $(GeSiO_2)Li^+Na^+$, $(GeSiO_2)Li^+K^+$, $(SnSiO_2)Li^+Na^+$, and $(SnSiO_2)Li^+K^+$ was carried out including using density functional theory (DFT) computations at the coulomb-attenuating method/Becke, 3-parameter, Lee–Yang–Parr [CAM–B3LYP–D3/6-311+G (d,p)] level of theory. The hypothesis of the ion-transporting phenomenon was confirmed by density distributions of charge density differences (CDD), total density of states (TDOS), and localized orbital locator (LOL) for nanoclusters of $(GeSiO_2)Li^+Na^+$, $(GeSiO_2)Li^+K^+$, $(SnSiO_2)Li^+Na^+$, and $(SnSiO_2)Li^+K^+$. The fluctuation in charge density values demonstrates that the electronic densities were mainly located at the boundary of adsorbate/adsorbent atoms during the adsorption status. The values detect that with adding lithium, sodium and potassium, the negative atomic charge of oxygen atoms of O_2, O_3, O_7–O_{12}, O_{14}, O_{15}, O_{17}, O_{18}, O_{22}–O_{27}, O_{29}, O_{30} in $(GeSiO_2)Li^+Na^+$, $(GeSiO_2)Li^+K^+$, $(SnSiO_2)Li^+Na^+$, and $(SnSiO_2)Li^+K^+$ nanoclusters augments as the advantages of lithium, sodium, or potassium over Ge, Sn/Si, they possess its higher electron and hole motion, allowing lithium, sodium or potassium instruments to operate at higher frequencies than Ge, Sn/Si instruments. Among these, sodium-ion transfer seems to show the most promise in terms of initial capacity. In fact, the counter map of LOL can confirm that $(GeSiO_2)Li^+Na^+$, $(GeSiO_2)Li^+K^+$, $(SnSiO_2)Li^+Na^+$, and $(SnSiO_2)Li^+K^+$ nanoclusters may increase the efficiency during ion transporting. This ion transport can create and maintain an electrochemical gradient, which is crucial for various cellular processes, including cell volume regulation, electrical excitability, and secondary active transport. The current study wants to delve deeper into several aspects of this molecular entity, such as describing its structure and mode of operation in atomic detail, understanding its molecular and functional diversity, and examining the consequences of its malfunction due to structural alterations.

Keywords: Cell membrane; Li^+Na^+ and Li^+K^+; ion transport, Ge/Sn/Si oxide; density of states.

1. Introduction

While prominently represented in the environment, lithium ions are not essential cofactors in biological systems [1–3]. In contrast, sodium, potassium, calcium, and magnesium are essential cofactors in multiple biological systems, and others, such as iron, zinc, and copper, play a role in some specific systems [4–7]. Thus, lithium ions appear to have been isolated from being incorporated as an essential element during the evolution of increasingly complex biological systems [8–13].

Irrespective of those who discovered Li salt's effects on patients with bipolar disorder, its use in these conditions became the standard for decades and continues today. In the treatment of bipolar disorder patients with lithium salts, it has been noted that not all patients are responsive to therapeutic doses of this intervention [14–23].

The nanomaterials, however, are widely applied in photocatalysis, energy, sensing, water purification, biomedicine, and electronics, with further material engineering for other future applications [24–28]. In fact, these are semiconductors in which the pure state of the semiconductor material is deliberately diluted by adding some quantities of impurities. By so doing, their conductivity and properties are improved as compared to the intrinsic semiconductors.

As the effect of Li salt utilization as a replacement for NaCl was an obvious failure, its successful usage in the remedy of bipolar disorder in patients was a stimulus from several outlooks for a more detailed research of Li salt's impacts on other biological systems, with the emergence of a better understanding of its broad significance in biology and its functions as a modulator or regulator of biological systems. It performs a very critical task in monitoring alterations in the system entirely owing to genetics or biological heterogeneity in humans [29–34].

Currently, the present research aims to explore the possibility of using $GeSiO_2$ and $SnSiO_2$ nanocages for ion transport of Li^+Na^+ and Li^+K^+ by employing first-principles calculations. We have analyzed the structural and electronic properties of $(GeSiO_2)Li^+Na^+$, $(GeSiO_2)Li^+K^+$, $(SnSiO_2)Li^+Na^+$, and $(SnSiO_2)Li^+K^+$ nanoclusters using state-of-the-art computational techniques.

2. Materials and Methods

Semiconductors are solid substances that are neither good conductors of metals nor insulators of glass, but have a crystalline structure and contain very few free electrons at room temperature. They have resistivities and energy gaps that lie between the conductors and insulators. The aim of this study is to transport alkali metal ions of Li^+, Na^+, K^+ by $(GeSiO_2)$ and $(SnSiO_2)$ nanocages towards the formation of $(GeSiO_2)Li^+Na^+$, $(GeSiO_2)Li^+K^+$, $(SnSiO_2)Li^+Na^+$, and $(SnSiO_2)Li^+K^+$ (Figure 1), which can increase the ion transfer in human cells. The Bader charge analysis [35] was discussed during ion transporting through the formation of $(GeSiO_2)Li^+Na^+$, $(GeSiO_2)Li^+K^+$, $(SnSiO_2)Li^+Na^+$, and $(SnSiO_2)Li^+K^+$ nanoclusters (Figure 1). The rigid potential energy surface using density functional theory [36–38] was performed due to the Gaussian 16 revision C.01 program package [39] and GaussView 6.1 [40]. The coordination input for ion transporting by $(GeSiO_2)Li^+Na^+$, $(GeSiO_2)Li^+K^+$, $(SnSiO_2)Li^+Na^+$, and $(SnSiO_2)Li^+K^+$ has been LANL2DZ and 6-311+G (d,p) basis sets.

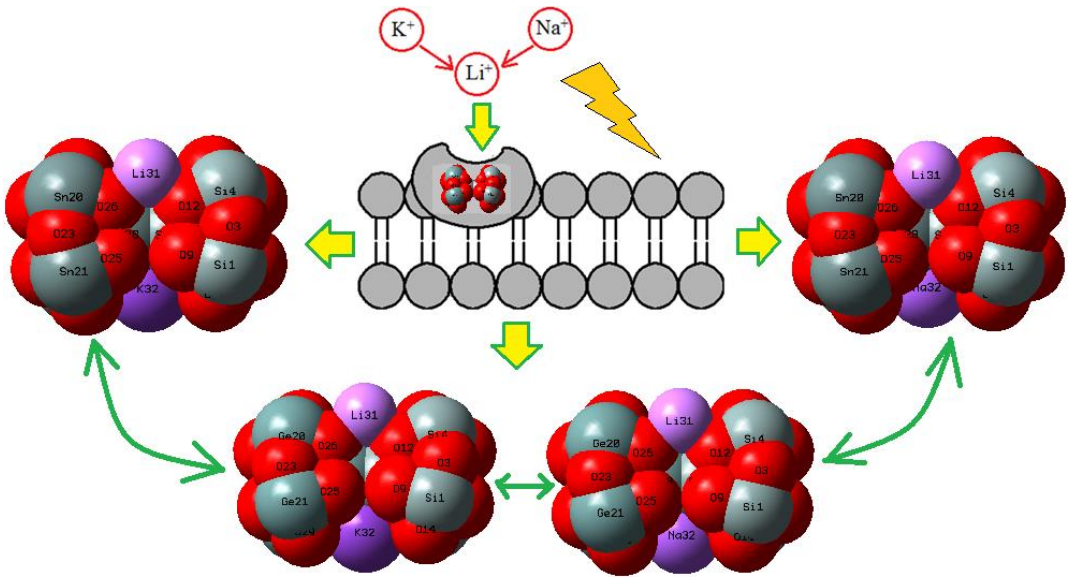

Figure 1. Ion Transport of Li^+, Na^+, K^+ across the cell membrane by (GeO–SiO) and (SnO–SiO) nanocages through formation of $(GeSiO_2)Li^+Na^+$, $(GeSiO_2)Li^+K^+$, $(SnSiO_2)Li^+Na^+$, $(SnSiO_2)Li^+K^+$ nanoclusters.

In our research, the calculations have been done by CAM–B3LYP–D3 /EPR–3 level of theory. The exact exchange energy functional is expressed in terms of the Kohn–Sham orbitals rather than the density, so it is termed an *implicit* density functional. One of the most commonly used versions is B3LYP, which stands for "Becke, 3-parameter, Lee–Yang–Parr" [41–43]. It was demonstrated that CAM-B3LYP yields saving energies of similar quality to those from B3LYP, while also performing well for charge transfer in a simulated model, which B3LYP underestimates enormously.

3. Results and Discussion

3.1. Charge density differences analysis.

The amounts of charge density differences (CDD) are measured by considering isolated atoms or noninteracting ones. The mentioned approximation can be the lightest to use because the superposition value may be received from the primary status of the self-consistency cycle in the code that carries out the density functional theory (Figure 2a, b, c, d) [44].

In Figure 2a, the $(GeSiO_2)Li^+Na^+$ cluster with the fluctuation in the region around -12 to +8 Bohr has been formed. Furthermore, the atoms of O_2, O_3, O_7–O_{12}, O_{14}, O_{15}, O_{17}, O_{18}, O_{22}–O_{27}, O_{29}, O_{30} from $(GeSiO_2)Li^+K^+$ (Figure 2b) have shown the fluctuation around -12 to +8 Bohr. In addition, the $(SnSiO_2)Li^+Na^+$ cluster with the fluctuation in the region around -12 to +8 Bohr (Figure 2c) has been observed. Besides, $(SnSiO_2)Li^+K^+$ cluster with the fluctuation in the region around -12 to +8 Bohr (Figure 2d) has been seen.

Atomic charge was discussed during ion transferring through the formation of $(GeSiO_2)Li^+Na^+$, $(GeSiO_2)Li^+K^+$, $(SnSiO_2)Li^+Na^+$, and $(SnSiO_2)Li^+K^+$ nanoclusters, respectively (Tables 1 and 2). The atomic charge of Si, Ge, Sn, O, and alkali metals of Li^+, Na^+, and K^+ transferred by $(GeSiO_2)$ and $(SnSiO_2)$ nanocages has been measured. The values detect that with adding lithium, sodium and potassium, the negative atomic charge of oxygen atoms of O_2, O_3, O_7–O_{12}, O_{14}, O_{15}, O_{17}, O_{18}, O_{22}–O_{27}, O_{29}, O_{30} in $(GeSiO_2)Li^+Na^+$, $(GeSiO_2)Li^+K^+$, $(SnSiO_2)Li^+Na^+$, and $(SnSiO_2)Li^+K^+$ nanoclusters augments. In fact, $(GeSiO_2)Li^+Na^+$, $(GeSiO_2)Li^+K^+$, $(SnSiO_2)Li^+Na^+$, and $(SnSiO_2)Li^+K^+$ nanoclusters have

shown more efficiency than ($GeSiO_2$) or ($SnSiO_2$) clusters [30] for admitting the electron from electron donors of H_{33}, H_{34}, H_{35}, and H_{36} (Tables 1 and 2).

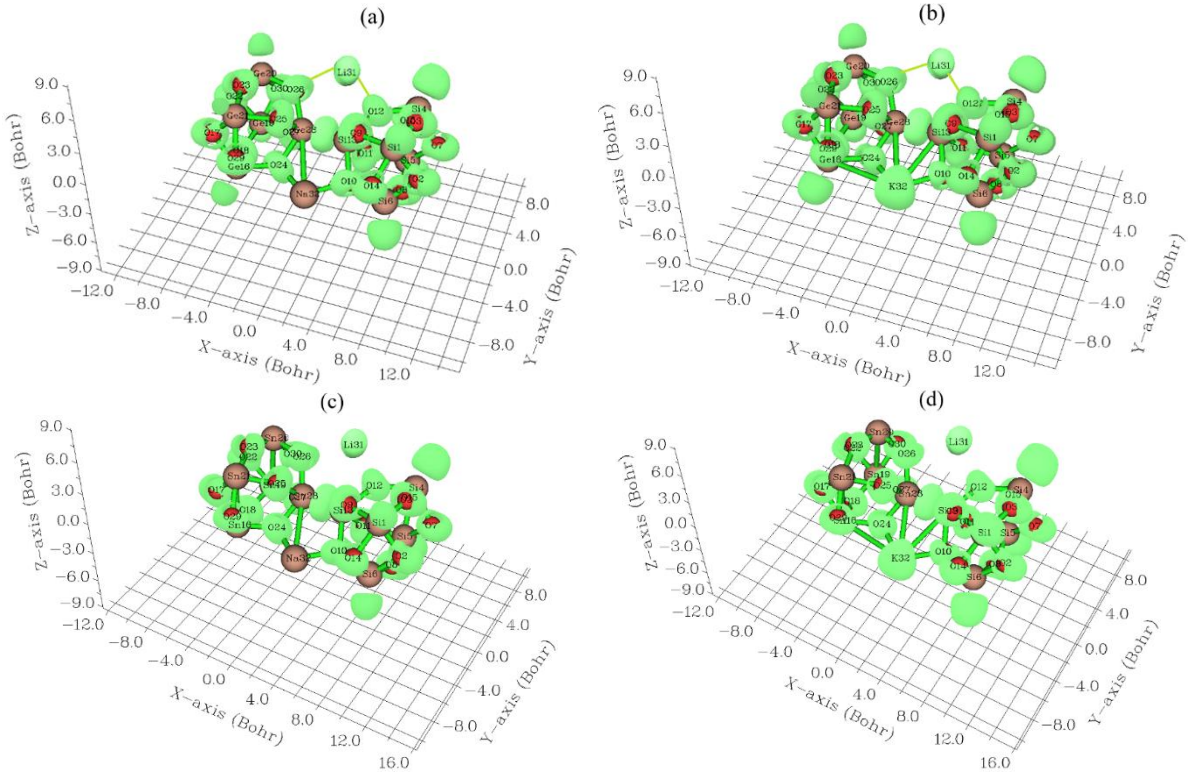

Figure 2. CDD graphs for **(a)** $(GeSiO_2)Li^+Na^+$; **(b)** $(GeSiO_2)Li^+K^+$; **(c)** $(SnSiO_2)Li^+Na^+$; **(d)** $(SnSiO_2)Li^+K^+$ nanoclusters.

Table 1. The atomic charge (Q/coulomb) for $(GeSiO_2)Li^+Na^+$ and $(GeSiO_2)Li^+K^+$ nanoclusters.

$(GeSiO_2)Li^+Na^+$		**$(GeSiO_2)Li^+K^+$**	
Atom	**Charge**	**Atom**	**Charge**
Si1	1.4620	Si1	1.4633
O2	–0.6577	O2	–0.6895
O3	–0.8351	O3	–0.8312
Si4	1.4288	Si4	1.4350
Si5	1.4499	Si5	1.46125
Si6	1.4581	Si6	1.4527
O7	–0.6825	O7	–0.6538
O8	–0.8429	O8	–0.8314
O9	–0.7903	O9	–0.7904
O10	–0.9988	O10	–1.0624
O11	–0.8024	O11	–0.8008
O12	–0.9533	O12	–0.9442
Si13	1.6394	Si13	1.6057
O14	–0.7323	O14	–0.7090
O15	–0.7257	O15	–0.7616
Ge16	1.4154	Ge16	1.3891
O17	–0.6523	O17	–0.6690
O18	–0.7795	O18	–0.7814
Ge19	1.4002	Ge19	1.3802
Ge20	1.3932	Ge20	1.3892
Ge21	1.4036	Ge21	1.3897
O22	–0.6668	O22	–0.6228
O23	–0.7840	O23	–0.7872
O24	–0.9600	O24	–1.0065
O25	–0.7804	O25	–0.7947
O26	–0.9081	O26	–0.9177
O27	–0.7872	O27	–0.7596
Ge28	1.2894	Ge28	1.2323
O29	–0.7393	O29	–0.7043
O30	–0.7193	O30	–0.7305
Li31	0.7412	Li31	0.7317

$(GeSiO_2)Li^+Na^+$		$(GeSiO_2)Li^+K^+$	
Atom	**Charge**	**Atom**	**Charge**
Na32	0.7169	K32	0.9183

Table 2. The atomic charge (Q/coulomb) for $(SnSiO_2)Li^+Na^+$ and $(SnSiO_2)Li^+K^+$ nanoclusters.

$(SnSiO_2)Li^+Na^+$		$(SnSiO_2)Li^+K^+$	
Atom	Charge	Atom	Charge
Si1	1.4606	Si1	1.4322
O2	–0.6356	O2	–0.6374
O3	–0.8304	O3	–0.8505
Si4	1.4116	Si4	1.3833
Si5	1.4378	Si5	1.4218
Si6	1.4628	Si6	1.4225
O7	–0.7260	O7	–0.6603
O8	–0.8371	O8	–0.8570
O9	–0.7879	O9	–0.7782
O10	–1.0023	O10	–1.0651
O11	–0.8100	O11	–0.8011
O12	–0.9499	O12	–0.9407
Si13	1.3977	Si13	1.3721
O14	–0.7674	O14	–0.7208
O15	–0.6972	O15	–0.7108
Sn16	1.6975	Sn16	1.6924
O17	–0.8093	O17	–0.8143
O18	–0.8830	O18	–0.8782
Sn19	1.6966	Sn19	1.6983
Sn20	1.6701	Sn20	1.6756
Sn21	1.6973	Sn21	1.7024
O22	–0.8446	O22	–0.8299
O23	–0.8928	O23	–0.8926
O24	–1.0672	O24	–1.1100
O25	–0.9083	O25	–0.9060
O26	–1.0000	O26	–0.9997
O27	–0.9326	O27	–0.9211
Sn28	1.8333	Sn28	1.7233
O29	–0.8900	O29	–0.8884
O30	–0.8596	O30	–0.8607
Li31	0.7052	Li31	0.7089
Na32	0.6609	K32	0.8901

3.2. TDOS analysis.

Squirming the molecular orbital data owing to Gaussian graphs of unit altitude and entire width at "half maximum (FWHM)" of 0.3 eV by "GaussSum 3.0.2" [45] have computed total density of states (TDOS) diagrams. Regarding ion transport behavior through formation of $(GeSiO_2)Li^+Na^+$, $(GeSiO_2)Li^+K^+$, $(SnSiO_2)Li^+Na^+$, and $(SnSiO_2)Li^+K^+$ nanoclusters, TDOS has been measured. This parameter can indicate the existence of important chemical interactions, often on the convex side (Figure 3a, b, c, d). During the formation of $(GeSiO_2)Li^+Na^+$ cluster, Figure 3a shows sharp and sophisticated peaks around –0.3, –0.45, and –0.60 a.u. Due to the covalent bond between two atoms of Li and Na with the $(GeSiO_2)$ cluster. $(GeSiO_2)Li^+K^+$ cluster has shown pointed peaks around –0.3, –0.45, and –0.60 a.u. Due to the covalent bond between two atoms of Li and K with the $(GeSiO_2)$ cluster (Figure 3b).

Furthermore, the maximum energy of TDOS for $(SnSiO_2)Li^+Na^+$ (Figure 3c) with several peaks around –0.30, –0.40, and –0.55 a.u., with a maximum density of state of ≈ 24 around –0.30 a.u., has been shown. Similar behavior of TDOS graphs has been observed for a hybrid cluster of $(SnSiO_2)Li^+K^+$ (Figure 3d) with several remarkable peaks around –0.30, –0.45, –0.55, and –0.7 a.u.

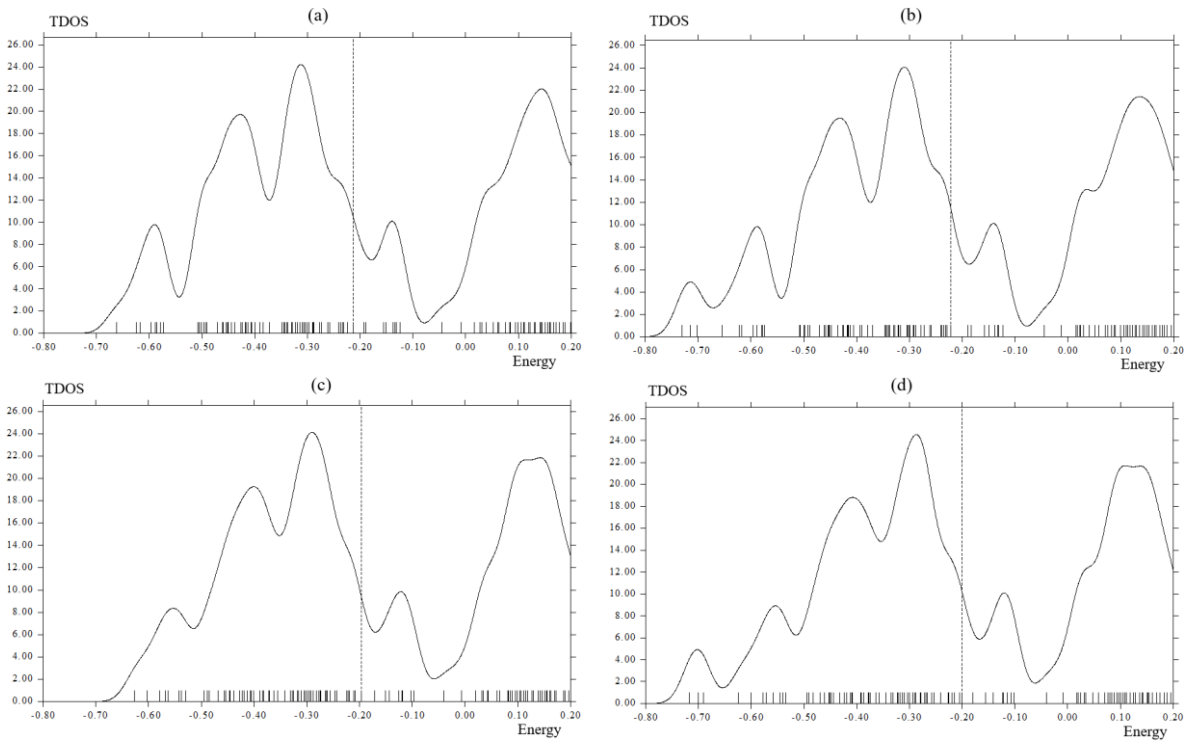

Figure3. TDOS graphs of **(a)** $(GeSiO_2)Li^+Na^+$; **(b)** $(GeSiO_2)Li^+K^+$; **(c)** $(SnSiO_2)Li^+Na^+$; **(d)** $(SnSiO_2)Li^+K^+$ nanoclusters.

3.3. LOL analysis.

The localized orbital locator (LOL) has a similar expression compared to the electron localization function (ELF) [46].

$$\mathrm{LOL(r)} = \frac{\tau(\mathrm{r})}{1+\tau(\mathrm{r})};\ \tau(\mathrm{r}) = \frac{D_0(\mathrm{r})}{\frac{1}{2}\sum_i \eta_i |\nabla\varphi_i\,(\mathrm{r})|^2} \quad (1)$$

$$D_0(\mathrm{r}) = \frac{3}{10}(6\pi^2)^{2/3}\left[\rho_\alpha\,(\mathrm{r})^{5/3} + \rho_\beta\,(\mathrm{r})^{5/3}\right] \quad (2)$$

Multiwfn [47, 48] also supports the approximate version of LOL defined by Tsirelson and Stash [49], namely, the actual kinetic energy term in LOL is replaced by second-order gradient expansion like ELF, which may demonstrate a broad span of bonding samples. This is Tsirelson's version of LOL, which can be activated by setting "ELFLOL_type" to 1. For a special reason, if "ELFLOL_type" in settings.ini is changed from 0 to 2, another formalism will be used:

$$\mathrm{LOL}(\mathbf{r}) = \frac{1}{1+\left[{}^{1}/_{\tau(\mathbf{r})}\right]^2} \quad (3)$$

If the parameter "ELFLOL_cut" in settings.ini is set to x, then LOL will be zero where LOL is less than *x*.

Ion transferring through the formation of $(GeSiO_2)Li^+Na^+$, $(GeSiO_2)Li^+K^+$, $(SnSiO_2)Li^+Na^+$, and $(SnSiO_2)Li^+K^+$ nanoclusters can be defined by LOL graphs owing to exploring their delocalization/localization characterizations of electrons and chemical bonds (Figure 4a,b,c,d) [50–53].

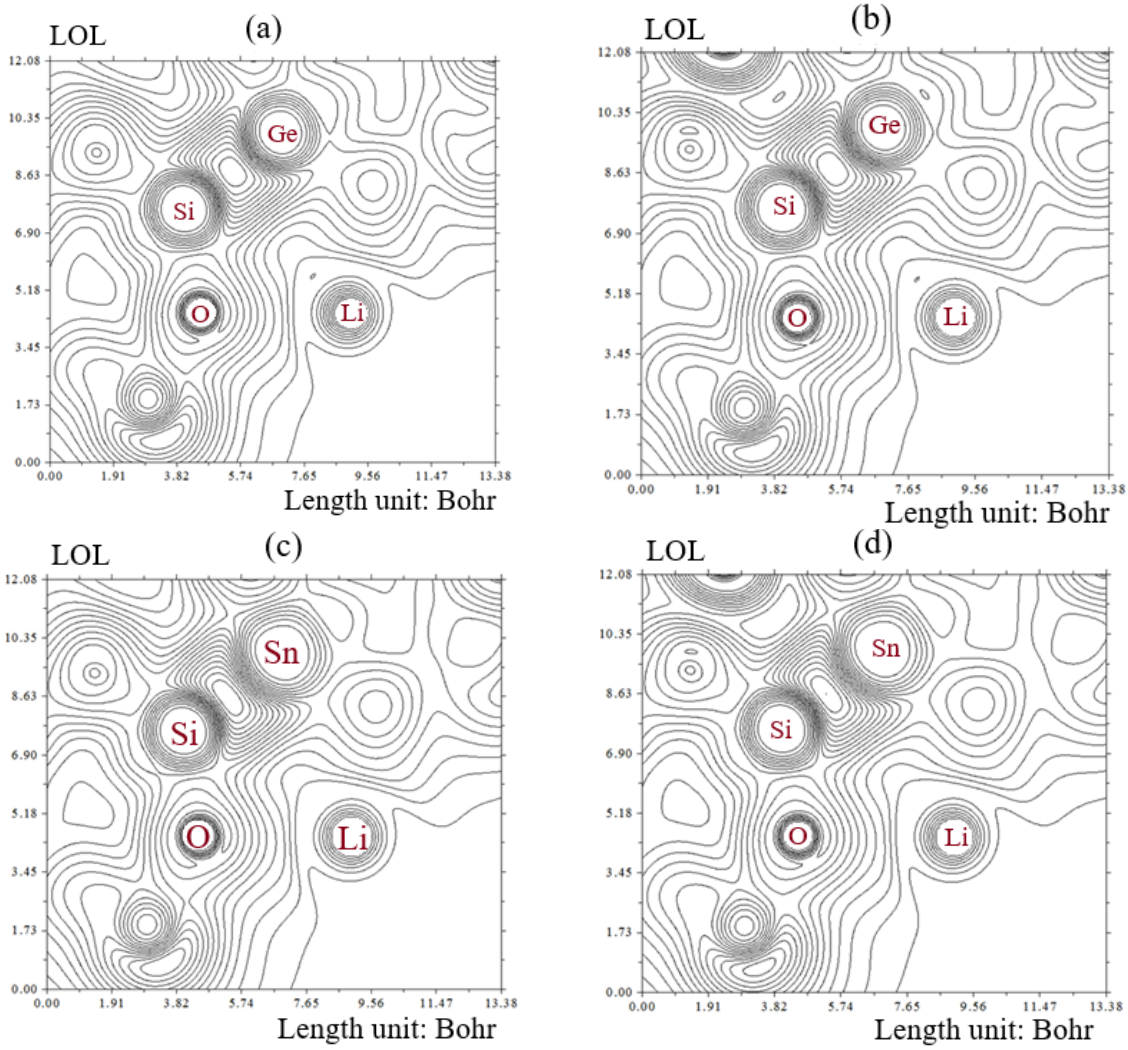

Figure 4. The counter map of LOL graphs for **(a)** $(GeSiO_2)Li^+Na^+$; **(b)** $(GeSiO_2)Li^+K^+$; **(c)** $(SnSiO_2)Li^+Na^+$; **(d)** $(SnSiO_2)Li^+K^+$ nanoclusters.

A vaster jointed area engaged by an isosurface map has shown the electron delocalization in $(GeSiO_2)Li^+Na^+$ (Figure 4a), $(GeSiO_2)Li^+K^+$ (Figure 4b), $(SnSiO_2)Li^+Na^+$ (Figure 4c), and $(SnSiO_2)Li^+K^+$ (Figure 4d) through labeling atoms of O12, Si13, O26, Ge28/Sn28, X31(X=Li, Na or K) and H35. In fact, the counter map of LOL can confirm that $(GeSiO_2)Li^+Na^+$, $(GeSiO_2)Li^+K^+$, $(SnSiO_2)Li^+Na^+$, and $(SnSiO_2)Li^+K^+$ nanoclusters may increase the efficiency during ion transporting.

Table 3. Dipole moment (debye), LUMO, HOMO, and energy gap (ΔE) for $(GeSiO_2)Li^+Na^+$, $(GeSiO_2)Li^+K^+$, $(SnSiO_2)Li^+Na^+$, and $(SnSiO_2)Li^+K^+$ heteroclusters.

Heteroclusters	Dipole moment (debye)	E_{HOMO} (eV)	E_{LUMO} (eV)	$\Delta E = E_{LUMO} - E_{HOMO}$ (eV)
$(GeSiO_2)Li^+Na^+$	2.0853	–5.8010	–5.2579	0.5431
$(GeSiO_2)Li^+K^+$	1.5622	–6.0315	–5.1446	0.8869
$(SnSiO_2)Li^+Na^+$	5.0772	–5.3386	–4.6734	0.6651
$(SnSiO_2)Li^+K^+$	6.4714	–5.4629	–4.9025	0.5604

Moreover, the intermolecular orbital overlap integral is important in discussions of intermolecular charge transfer, which can calculate HOMO-HOMO and LUMO-LUMO overlap integrals between the H_2 molecules and heteroclusters of $(GeSiO_2)Li^+Na^+$, $(GeSiO_2)Li^+K^+$, $(SnSiO_2)Li^+Na^+$, and $(SnSiO_2)Li^+K^+$. The applied wavefunction level is CAM–B3LYP–D3/6–311+G (d, p) that corresponds to HOMO and LUMO, respectively (Table 3).

The amount of "Mayer bond order" [54] is generally according to the empirical bond order for the single bond, which is nearly 1.0. "Mulliken bond order" [55] with a small accord with empirical bond order is not appropriate for quantifying bonding strength, for which Mayer bond order always performs better. However, "Mulliken bond order" is a good qualitative indicator for "positive amount" of bonding and "negative amount" of antibonding, which are evacuated and localized, respectively (Table 4).

Table 4. The bond order of Mayer, Wiberg, Mulliken, Laplacian, and Fuzzy from mixed alpha and beta density matrix for $(GeSiO_2)Li^+Na^+$, $(GeSiO_2)Li^+K^+$, $(SnSiO_2)Li^+Na^+$, $(SnSiO_2)Li^+K^+$ heteroclusters.

Compound	Bond type	Bond order				
		Mayer	Wiberg	Mulliken	Laplacian	Fuzzy
$(GeSiO_2)Li^+Na^+$	O12–Si13	0.4916	0.6121	0.1901	0.2102	1.0149
	O12–Li31	0.1405	0.2054	0.1300	0.1586	0.1336
	O26–Li31	0.2116	0.2732	0.1830	0.2032	0.1789
	O26–Ge28	0.6388	0.5733	0.2466	0.2395	1.0434
	Si13–Ge28	0.6316	0.7527	0.6785	2.2836	0.8317
	O10–Si13	0.4359	0.6018	0.1239	0.1413	0.9110
	O10–Na32	0.2471	0.2257	0.2669	0.0769	0.6335
	O24–Na32	0.2410	0.2190	0.2704	0.0516	0.5598
	O24–Ge28	0.3621	0.5564	0.0856	0.2491	0.9539
$(GeSiO_2)Li^+K^+$	O12–Si13	0.4993	0.6182	0.2012	0.2180	1.0213
	O12–Li31	0.1391	0.2037	0.1272	0.1352	0.1315
	O26–Li31	0.2176	0.2772	0.1865	0.1941	0.1808
	O26–Ge28	0.4995	0.5838	0.2581	0.2438	1.0562
	Si13–Ge28	0.7024	0.7860	0.5475	2.3676	0.8538
	O10–Si13	0.4299	0.5954	0.0842	0.1291	0.9012
	O10–K32	0.7510	0.2648	0.5656	0.1557	0.7332
	O24–K32	0.7482	0.2571	0.4638	0.1139	0.6526
	O24–Ge28	0.3791	0.5496	0.4175	0.1876	0.9399
$(SnSiO_2)Li^+Na^+$	O12–Si13	0.4878	0.6031	0.1784	0.2050	1.0002
	O12–Li31	0.1555	0.2119	0.1375	0.1649	0.1361
	O26–Li31	0.2463	0.2824	0.1984	0.1419	0.1564
	O26–Sn28	0.4561	0.5295	0.2540	0.4585	1.2026
	Si13–Sn28	0.7026	0.7441	1.1803	2.7926	0.8697
	O10–Si13	0.4683	0.6055	0.1788	0.1454	0.9075
	O10–Na32	0.2639	0.2228	0.2881	0.0748	0.6292
	O24–Na32	0.2766	0.2204	0.2932	0.0512	0.4983
	O24–Sn28	0.3222	0.1834	0.1101	0.4097	1.1118
$(SnSiO_2)Li^+K^+$	O12–Si13	0.5046	0.6117	0.1850	0.2144	1.0107
	O12–Li31	0.1562	0.2052	0.1395	0.1547	0.1341
	O26–Li31	0.2444	0.2795	0.1985	0.1389	0.1555
	O26–Sn28	0.4623	0.5316	0.2627	0.4579	1.2047
	Si13–Sn28	0.7559	0.7660	1.0806	2.8159	0.8750
	O10–Si13	0.4534	0.6007	0.1356	0.1308	0.9043
	O10–K32	0.1682	0.2583	0.5401	0.1497	0.7255
	O24–K32	0.1632	0.2524	0.4742	0.0739	0.5838
	O24–Sn28	0.3677	0.5234	0.0808	0.3946	1.0985

As shown in Table 4, the "Laplacian bond order" [56] exhibits a direct correlation with bond polarity, bond dissociation energy, and bond vibrational frequency. The low value of the Laplacian bond order might demonstrate that it is insensitive to the calculation degree applied for producing electron density [57–63].

Generally, the value of “Fuzzy bond order” is near Mayer bond order, especially for low-polar bonds, but is much more stable with respect to the change in basis set. Computation of "Fuzzy bond order" demands running "Becke's DFT" numerical integration, owing to which the calculation value is larger than the assessment of "Mayer bond order", and it can be more precise [64].

4. Conclusions

In this work, we have investigated the ion transporting of Li^+, Na^+, K^+ by (GeO–SiO) and (SnO–SiO) heteroclusters in the human cell through the formation of $(GeSiO_2)Li^+Na^+$, $(GeSiO_2)Li^+K^+$, $(SnSiO_2)Li^+Na^+$, $(SnSiO_2)Li^+K^+$ heteroclusters by first-principles computations of the DFT method. The alterations of charge density illustrated a remarkable charge transfer towards $(GeSiO_2)Li^+Na^+$, $(GeSiO_2)Li^+K^+$, $(SnSiO_2)Li^+Na^+$, $(SnSiO_2)Li^+K^+$. The fluctuation in charge density values demonstrates that the electronic densities were at the boundary of adsorbate/adsorbent atoms during the ion-transporting status. Besides, thermodynamic parameters describing ion transporting through the formation of alkali metals-based nanoclusters of $(GeSiO_2)Li^+Na^+$, $(GeSiO_2)Li^+K^+$, $(SnSiO_2)Li^+Na^+$, $(SnSiO_2)Li^+K^+$ have been investigated, including the internal process of the adsorbent–adsorbate system. Finally, the chemical tailorability and size design or reduction into quantum dots are some of the features that are constantly explored for newer applications. There are various methods that have been applied in the preparation of the different semiconductor nanomaterials. The relative efficacies and cation selectivities of polyvalent anions can largely be explained on the basis of electrostatic interactions governing ion pair formation. However, the chelating properties, structural flexibility, polarizability of the anions, and the accessibility of the ion pairs to the anion exchange pathway also need to be considered.

Author Contributions

Conceptualization, F.M.; methodology, F.M.; software, F.M.; validation, F.M.; formal analysis, F.M.; investigation, F.M.; resources, F.M.; data curation, F.M.; writing—original draft preparation, F.M.; writing—review and editing, F.M.; visualization, F.M.; supervision, F.M.; project administration, F.M.; funding acquisition, F.M. The author has read and agreed to the published version of the manuscript.

Institutional Review Board Statement

Not applicable.

Informed Consent Statement

Not applicable.

Data Availability Statement

Not applicable.

Funding

This research received no external funding.

Acknowledgments

In successfully completing this paper and its research, the author is grateful to Kastamonu University.

Conflict of Interest

The author declares no conflict of interest.

References

1. Naeem, A.; Aslam, M.; Saifullah; Muhling, K.H. Lithium: Perspectives of nutritional beneficence, dietary intake, biogeochemistry, and biofortification of vegetables and mushrooms. *Sci. Total Environ.* **2021**, *798*, 149249, https://doi.org/10.1016/j.scitotenv.2021.149249.
2. Shahriari, S.; Mollaamin, F.; Monajjemi, M. Increasing the Performance of {[(1-x-y) $LiCo_{0.3}Cu_{0.7}$] (Al and Mg doped)] O_2}, xLi_2MnO_3, $yLiCoO_2$ Composites as Cathode Material in Lithium-Ion Battery: Synthesis and Characterization. *Micromachines* **2024**, *14*, 241, https://doi.org/10.3390/mi14020241.
3. Hart, D.A. Lithium Ions as Modulators of Complex Biological Processes: The Conundrum of Multiple Targets, Responsiveness and Non-Responsiveness, and the Potential to Prevent or Correct Dysregulation of Systems during Aging and in Disease. *Biomolecules* **2024**, *14*, 905, https://doi.org/10.3390/biom14080905.
4. Dobosy, P.; Illés, Á.; Endrédi, A.; Záray, G. Lithium concentration in tap water, bottled mineral water, and Danube River water in Hungary. *Scientific Reports* **2023**, *13*, 12543, https://doi.org/10.1038/s41598-023-38864-6.
5. De-Paula, V.J.; Forlenza, O.V. Lithium modulates multiple tau kinases with distinct effects in cortical and hippocampal neurons according to concentration ranges. *Naunyn-Schmiedeberg's Arch Pharmacol* **2022**, *395*, 105–113, https://doi.org/10.1007/s00210-021-02171-6.
6. Osete, J.R.; Akkouh, I.A.; Ievglevskyi, O.; Vandenberghe, M.; de Assis, D.R.; Ueland, T.; Kondratskaya, E.; Holen, B.; Szabo, A.; Hughes, T. Transcriptional and functional effects of lithium in bipolar disorder iPSC-derived cortical spheroids. *Molecular Psychiatry* **2023**, *28*, 3033-3043, https://doi.org/10.1038/s41380-023-01944-0.
7. Salem, D.; Fecek, R.J. Role of microtubule actin crosslinking factor 1 (MACF1) in bipolar disorder pathophysiology and potential in lithium therapeutic mechanism. *Transl. Psychiatry* 2023, *13*, 221, https://doi.org/10.1038/s41398-023-02483-6.
8. Monajjemi, M.; Razavian, M.; Mollaamin, F.; Naderi, F.; Honarparvar, B. A theoretical thermochemical study of solute-solvent dielectric effects in the displacement of codon-anticodon base pairs. *Russian Journal of Physical Chemistry A, Focus on Chemistry* **2008**, *82*, 2277-2285, https://doi.org/10.1134/S0036024408130207.
9. Khalili Hadad, B.; Mollaamin, F.; Monajjemi, M. Biophysical chemistry of macrocycles for drug delivery: A theoretical study. *Russian chemical bulletin* **2011**, *60*, 238-241, https://doi.org/10.1007/s11172-011-0039-5.
10. Monajjemi, M.; Noei, M.; Mollaamin, F. Design of fMet-tRNA and calculation of its bonding properties by quantum mechanics. *Nucleosides Nucleotides Nucleic Acids.* **2010**, *29*, 676-83, https://doi.org/10.1080/15257771003781642.
11. Mollaamin, F. Computational Methods in the Drug Delivery of Carbon Nanocarriers onto Several Compounds in Sarraceniaceae Medicinal Plant as Monkeypox Therapy. *Computation* **2023**, *11*, 84. https://doi.org/10.3390/computation11040084.
12. Mollaamin, F.; Monajjemi, M. In Situ Ti-Embedded SiC as Chemiresistive Nanosensor for Safety Monitoring of CO, CO_2, NO, NO_2: Molecular Modelling by Conceptual Density Functional Theory. *Russ. J. Phys. Chem. B.* **2024**, *18*, 49-66, https://doi.org/10.1134/S1990793124010159.
13. Mollaamin, F. Features of parametric point nuclear magnetic resonance of metals implantation on boron nitride nanotube by density functional theory/electron paramagnetic resonance. *J. Comput. Theor. Nanosci.* **2014**, *11*, 2393-2398, https://doi.org/10.1166/jctn.2014.3653.
14. Amare, A.T.; Thalamuthu, A.; Schubert, K.O.; Fullerton, J.M.; Ahmed, M.; Hartmann, S.; Papiol, S.; Heilbronner, U.; Degenhardt, F.; Tekola-Ayele, F. Association of polygenic score and the involvement of cholinergic and glutamatergic pathways with lithium treatment response in patients with bipolar disorder. *Molecular psychiatry* **2023**, *28*, 5251-5261, https://doi.org/10.1038/s41380-023-02149-1.
15. Diaz-Zuluaga, A.M.; Velez, J.I.; Cuartas, M.; Valencia, J.; Castano, M.; Palacio, J.D.; Arcos-Burgos, M.; Lopez-Jaramillo, C. Ancestry component as a major predictor of lithium response in the treatment of bipolar disorder. *J. Affect. Disord.* **2023**, *332*, 203–209. https://doi.org/10.1016/j.jad.2023.03.058.

16. Monajjemi, M.; Khaleghian, M.; Tadayonpour, N.; Mollaamin, F. The effect of different solvents and temperatures on stability of single-walled carbon nanotube: A QM/MD study. *International Journal of Nanoscience* **2010**, *9*, 517-529, https://doi.org/10.1142/S0219581X10007071.
17. Herrera-Rivero, M.; Gutierrez-Fragosa, K. International consortium on lithium genetics (ConLi + Gen); Kurtz, J.; Baune, B.T. Immunogenetics of lithium response and psychiatric phenotypes in patients with bipolar disorder. *Transl. Psychiatry* **2024**, *14*, 174, https://doi.org/10.1038/s41398-024-02865-4.
18. Mollaamin, F.; Mohammadi, S.; Khalaj, Z.; Monajjemi, M. Computational Modelling of Boron Nitride Nanosheet for Detecting and Trapping of Water Contaminant. *Russ. J. Phys. Chem. B.* **2024**, *18*, 67-82, https://doi.org/10.1134/S1990793124010330.
19. Bellinger, D.C. Lithium in drinking water-a novel environmental risk factor for autism spectrum disorder? *JAMA Pediatr.* **2023**, *177*, 563–564, https://doi.org/10.1001/jamapediatrics.2023.0330.
20. Monajjemi, M.; Karachi, N.; Mollaamin, F. The investigation of sequence-dependent interaction of messenger RNA binding to carbon nanotube. *Fullerenes, Nanotubes and Carbon Nanostructures.* **2014**, *22*, 643–662, https://doi.org/10.1080/1536383X.2012.717557.
21. Pisanu, C.; Meloni, A.; Severino, G.; Squassina, A. Genetic and Epigenetic Markers of Lithium Response. *Int. J. Mol. Sci.* **2022**, *23*, 1555, https://doi.org/10.3390/ijms23031555.
22. Bopp, S.K.; Heilbronner, U.; Schlattmann, P.; Buspavanich, P.; Lang, U.E.; Heinz, A.; Schulze, T.G.; Adli, M.; Muhleisen, T.W.; Ricken, R. A GWAS top hit for circulating leptin is associated with weight gain but not with leptin protein levels in lithium-augmented patients with major depression. *Eur. Neuropsychopharmacol.* **2021**, *53*, 114–119, https://doi.org/10.1016/j.euroneuro.2021.09.007.
23. Zafrilla-Lopez, M.; Acosta-Diez, M.; Mitjans, M.; Gimenez-Palomo, A.; Saiz, P.A.; Barrot-Feixat, C.; Jimenez, E.; Papiol, S.; Ruiz, V.; Gavin, P. Lithium response in bipolar disorder: Epigenome-wide DNA methylation signatures and epigenetic aging. *European Neuropsychopharmacology* **2024**, *85*, 23, https://doi.org/10.1016/j.euroneuro.2024.03.010.
24. Mollaamin, F.; Monajjemi, M. Nanomaterials for Sustainable Energy in Hydrogen-Fuel Cell: Functionalization and Characterization of Carbon Nano-Semiconductors with Silicon, Germanium, Tin or Lead through Density Functional Theory Study. *Russ. J. Phys. Chem. B.* **2024**, *18*, 607–623, https://doi.org/10.1134/S1990793124020271.
25. Mollaamin, F.; Shahriari, S.; Monajjemi, M. Influence of Transition Metals for Emergence of Energy Storage in Fuel Cells through Hydrogen Adsorption on the MgAl Surface. *Russ. J. Phys. Chem. B.* **2024**, *18*, 398–418, https://doi.org/10.1134/S199079312402026X.
26. Mollaamin, F. Competitive Intracellular Hydrogen-nanocarrier Among Aluminum, Carbon, or Silicon Implantation: a Novel Technology of Eco-Friendly Energy Storage using Research Density Functional Theory. Russ. *J. Phys. Chem. B.* **2024**, *18*, 805–820, https://doi.org/10.1134/S1990793124700131.
27. Mollaamin, F.; Monajjemi, M. Adsorption ability of Ga_5N_{10} nanomaterial for removing metal ions contamination from drinking water by DFT. *Int J Quantum Chem* **2024**, *124*, e27348, https://doi.org/10.1002/qua.27348.
28. Mollaamin, F.; Monajjemi, M. Structural, Electromagnetic and Thermodynamic Analysis of Ion Pollutants Adsorption in Water by Gallium Nitride Nanomaterial: a Green Chemistry Application. *Russ. J. Phys. Chem. B.* **2024**, *18*, 533-548, https://doi.org/10.1134/S199079312402012X.
29. Calabrese, E.J.; Pressman, P.; Hayes, A.W.; Dhawan, G.; Kapoor, R.; Agathokleous, E.; Calabrese, V. Lithium and hormesis: Enhancement of adaptive responses and biological performance via hermetic mechanisms. *J. Trace Elem. Med. Biol.* **2023**, *78*, 127156, https://doi.org/10.1016/j.jtemb.2023.127156.
30. Munteanu, C.; Rotariu, M.; Turnea, M.; Tătăranu, L.G.; Dogaru, G.; Popescu, C.; Spînu, A.; Andone, I.; Ionescu, E.V.; Țucmeanu, R.E. Lithium biological action mechanisms after ischemic stroke. *Life* **2022**, *12*, 1680, https://doi.org/10.3390/life12111680.
31. Anand, A.; Nakamura, K.; Spielberg, J.M.; Cha, J.; Karne, H.; Hu, B. Integrative analysis of lithium treatment associated effects on brain structure and peripheral gene expression reveals novel molecular insights into mechanism of action. *Translational Psychiatry* **2020**, *10*, 103, https://doi.org/10.1038/s41398-020-0784-z.
32. Rijal, S.; Jang, S.H.; Park, S.J.; Han, S.K. Lithium Enhances the GABAergic Synaptic Activities on the Hypothalamic Preoptic Area (hPOA) Neurons. *Int. J. Mol. Sci.* **2021**, *22*, 3908. https://doi.org/10.3390/ijms22083908.
33. Chen, S.; Underwood, B.R.; Jones, P.B.; Lewis, J.R.; Cardinal, R.N. Association between lithium use and the incidence of dementia and its subtypes: A retrospective cohort study. *PLoS Med.* **2022**, *19*, e1003941, https://doi.org/10.1371/journal.pmed.1003941.

34. Palmos, A.B.; Duarte, R.R.; Smeeth, D.M.; Hedges, E.C.; Nixon, D.F.; Thuret, S.; Powell, T.R. Lithium treatment and human hippocampal neurogenesis. *Translational psychiatry* **2021**, *11*, 555, https://doi.org/10.1038/s41398-021-01695-y
35. Henkelman,G.; Arnaldsson, A.; Jónsson, H. A fast and robust algorithm for Bader decomposition of charge density. *Computational Materials Science*. **2006**, *36*, 354–360, https://doi.org/10.1016/j.commatsci.2005.04.010.
36. Mollaamin, F.; Monajjemi, M. Adsorption ability of Ga_5N_{10} nanomaterial for removing metal ions contamination from drinking water by DFT. *Int J Quantum Chem*. **2024**, *124*, e27348, https://doi.org/10.1002/qua.27348.
37. Mollaamin, F.; and Monajjemi, M. Molecular modelling framework of metal-organic clusters for conserving surfaces: Langmuir sorption through the TD-DFT/ONIOM approach. *Molecular Simulation* **2023**, *49*, 365–376, https://doi.org/10.1080/08927022.2022.2159996.
38. Vosko, S. H.; Wilk, L.; Nusair, M. Accurate spin-dependent electron liquid correlation energies for local spin density calculations: a critical analysis. *Can. J. Phys*. **1980**, *58*, 1200–1211, https://doi.org/10.1139/p80-159.
39. Frisch, M.J.; Trucks, G.W.; Schlegel, H.B.; Scuseria, G.E.; Robb, M.A.; Cheeseman, J.R.; Scalmani, G.; Barone, V.; Petersson, G.A.; Nakatsuji, H.; Li, X.; Caricato, M.; Marenich, A.V.; Bloino, J.; Janesko, B.G.; Gomperts, R.; Mennucci, B.; Hratchian, H.P.; Ortiz, J. V.; Izmaylov, A. F.; Sonnenberg, J.L.; Williams-Young, D.; Ding, F.; Lipparini, F.; Egidi, F.; Goings, J.; Peng, B.; Petrone, A.; Henderson, T.; Ranasinghe, D.; Zakrzewski, V.G.; Gao, J.; Rega, N.; Zheng, G.; Liang, W.; Hada, M.; Ehara, M.; Toyota, K.; Fukuda, R.; Hasegawa, J.; Ishida, M.; Nakajima, T.; Honda, Y.; Kitao, O.; Nakai, H.; Vreven, T.; Throssell, K.; Montgomery, J.A., Jr.; Peralta, J.E.; Ogliaro, F.; Bearpark, M.J.; Heyd, J.J.; Brothers, E.N.; Kudin, K.N.; Staroverov, V.N.; Keith, T.A.; Kobayashi, R.; Normand, J.; Raghavachari, K.; Rendell, A.P.; Burant, J.C.; Iyengar, S.S.; Tomasi, J.; Cossi, M.; Millam, J.M.; Klene, M.; Adamo, C.; Cammi, R.; Ochterski, J.W.; Martin, R.L.; Morokuma, K.; Farkas, O.; Foresman, J.B.; Fox, D.J. Gaussian 16, Revision C.01, Gaussian, Inc., Wallingford CT, **2016**.
40. Dennington, R.; Keith, T.A.; Millam, J.M. GaussView 6.0. 16; Semichem Inc., Shawnee Mission, **2016**.
41. Mollaamin, F.; Monajjemi, M. Doping of Graphene Nanostructure with Iron, Nickel and Zinc as Selective Detector for the Toxic Gas Removal: A Density Functional Theory Study. *C-Journal of Carbon Research*. **2023**, *9*, 20, https://doi.org/10.3390/c9010020.
42. Mollaamin, F.; Monajjemi, M. Trapping of toxic heavy metals from water by GN–nanocage: Application of nanomaterials for contaminant removal technique. *J. Mol. Struct.* **2024**, *1300*, 137214, https://doi.org/10.1016/j.molstruc.2023.137214.
43. Mollaamin, F.; Monajjemi, M. Tribocorrosion Framework of (Iron, Nickel, Zinc)-Doped Graphene Nanosheet: New Sights into Sulfur Dioxide and Hydrogen Sulfide Removal Using DFT/TD-DFT Methods. *J Bio Tribo Corros.* **2023**, *9*, 47, https://doi.org/10.1007/s40735-023-00768-3.
44. Xu, Z.; Qin, C.; Yu, Y.; Jiang, G.; Zhao, L. First-principles study of adsorption, dissociation, and diffusion of hydrogen on α-U (110) surface. *AIP Advances* **2024**, *14*, 055114, https://doi.org/10.1063/5.0208082.
45. O'Boyle, N.M.; Tenderholt, A.L.; Langner, K.M. Cclib: a library for package-independent computational chemistry algorithms. *Journal of Computational Chemistry* **2008**, *29*, 839-845, https://doi.org/10.1002/jcc.20823.
46. Schmider, H.; Becke, A. Chemical content of the kinetic energy density. *Journal of Molecular Structure: THEOCHEM* **2000**, *527*, 51-61, https://doi.org/10.1016/S0166-1280(00)00477-2.
47. Lu, T.; Chen, F. Multiwfn: A multifunctional wavefunction analyzer. *Journal of Computational Chemistry* **2012**, *33*, 580-592, https://doi.org/10.1002/jcc.22885.
48. Tian, Lu. A comprehensive electron wavefunction analysis toolbox for chemists, Multiwfn. *J. Chem. Phys.* **2024**, *161*, 082503, https://doi.org/10.1063/5.0216272.
49. Tsirelson, V.; Stash, A. Analyzing experimental electron density with the localized-orbital locator. *Structural Science* **2002**, *58*, 780-785, https://doi.org/10.1107/S0108768102012338.
50. Mollaamin, F.; Monajjemi, M. Transition metal (X = Mn, Fe, Co, Ni, Cu, Zn)-doped graphene as gas sensor for CO_2 and NO_2 detection: a molecular modeling framework by DFT perspective. *J Mol Model.* **2023**, *29*, 119, https://doi.org/10.1007/s00894-023-05526-3.
51. Mollaamin, F.; Shahriari, S.; Monajjemi, M.; Khalaj, Z. Nanocluster of aluminum lattice via organic inhibitors coating: a study of Freundlich adsorption. *Journal of Cluster Science* **2023**, *34*, 1547-1562, https://doi.org/10.1007/s10876-022-02335-1.

52. Mollaamin, F.; Monajjemi, M. Tailoring and functionalizing the graphitic-like GaN and GaP nanostructures as selective sensors for NO, NO_2, and NH_3 adsorbing: a DFT study. *J Mol Model.* **2023**, *29*, 170, https://doi.org/10.1007/s00894-023-05567-8.
53. Mollaamin, F.; Monajjemi, M. In Silico-DFT Investigation of Nanocluster Alloys of Al-(Mg, Ge, Sn) Coated by Nitrogen Heterocyclic Carbenes as Corrosion Inhibitors. *J Clust Sci.* **2023**, *34*, 2901–2918, https://doi.org/10.1007/s10876-023-02436-5.
54. Mayer, I. Improved definition of bond orders for correlated wave functions. *Chemical Physics Letters* **2012**, *544*, 83-86, https://doi.org/10.1016/j.cplett.2012.07.003.
55. Mollaamin, F.; Ilkhani, A.; Sakhaei, N.; Bonsakhteh, B.; Faridchehr, A.; Tohidi, S.; Monajjemi, M. Thermodynamic and solvent effect on dynamic structures of nano bilayer-cell membrane: Hydrogen bonding study. *Journal of Computational and Theoretical Nanoscience* **2015**, *12*, 3148-3154, https://doi.org/10.1166/jctn.2015.4092.
56. Lu, T.; Chen, F. Bond order analysis based on the Laplacian of electron density in fuzzy overlap space. *The Journal of Physical Chemistry A* **2013**, *117*, 3100-3108, https://doi.org/10.1021/jp4010345.
57. Mollaamin, F.; Monajjemi, M. Graphene-based resistant sensor decorated with Mn, Co, Cu for nitric oxide detection: Langmuir adsorption & DFT method. *Sensor Review*. **2023**, *43*, 266–279. https://doi.org/10.1108/SR-03-2023-0040.
58. Mollaamin, F.; Monajjemi, M. Electric and Magnetic Evaluation of Aluminum–Magnesium Nanoalloy Decorated with Germanium Through Heterocyclic Carbenes Adsorption: A Density Functional Theory Study. *Russ. J. Phys. Chem. B.* **2023**, *17*, 658–672, https://doi.org/10.1134/S1990793123030223.
59. Mollaamin, F.; Monajjemi, M. Corrosion Inhibiting by Some Organic Heterocyclic Inhibitors Through Langmuir Adsorption Mechanism on the Al-X (X = Mg/Ga/Si) Alloy Surface: A Study of Quantum Three-Layer Method of CAM-DFT/ONIOM. *J Bio Tribo Corros.* **2023**, *9*, 33, https://doi.org/10.1007/s40735-023-00751-y.
60. Mollaamin, F.; Monajjemi, M. Graphene Embedded with Transition Metals for Capturing Carbon Dioxide: Gas Detection Study Using QM Methods. *Clean Technol.* **2023**, *5*, 403-417, https://doi.org/10.3390/cleantechnol5010020.
61. Mollaamin, F.; Monajjemi, M. Application of DFT and TD-DFT on Langmuir Adsorption of Nitrogen and Sulfur Heterocycle Dopants on an Aluminum Surface Decorated with Magnesium and Silicon. *Computation.* **2023**, *11*, 108, https://doi.org/10.3390/computation11060108.
62. Mollaamin, F.; Monajjemi, M. Carbon Nanotubes as Biosensors for Releasing Conjugated Bisphosphonates–Metal Ions in Bone Tissue: Targeted Drug Delivery through the DFT Method. *C-Journal of Carbon Research.* **2023**, *9*, 61, https://doi.org/10.3390/c9020061.
63. Mollaamin, F.; Monajjemi, M. Application of DFT/TD-DFT Frameworks in the Drug Delivery Mechanism: Investigation of Chelated Bisphosphonate with Transition Metal Cations in Bone Treatment. *Chemistry.* **2023**, *5*, 365-380, https://doi.org/10.3390/chemistry5010027.
64. Wang, X.; Zhang, X.; Pedrycz, W.; Yang, S.-H.; Boutat, D. Consensus of T-S Fuzzy Fractional-Order, Singular Perturbation, Multi-Agent Systems. *Fractal Fract.* **2024**, *8*, 523, https://doi.org/10.3390/fractalfract8090523.

Publisher's Note & Disclaimer